Relaxation of Dipolar-Coupled Spins in Transverse Fields : The role of Double-flip Processes

C. Pellet-Mary[1], M. Perdriat[1], P. Huillery[2], G. Hétet[1]

[1] *Laboratoire De Physique de l'École Normale Supérieure, École Normale Supérieure, PSL Research University, CNRS, Sorbonne Université, Université Paris Cité , 24 rue Lhomond, 75231 Paris Cedex 05, France*

[2] *Univ Rennes, INSA Rennes, CNRS, Institut FOTON - UMR 6082, F-35000 Rennes, France*

We study relaxation processes in dipolar-coupled negatively charged nitrogen vacancy (NV^-) centers under transverse electric fields and magnetic fields. Specifically, we uncover regimes where flip-flop, double-flip processes as well as mixing induced by local electric fields play a significant role in NV-NV cross-relaxation. Our results are relevant for understanding decoherence in many-body spin systems as well as for high sensitivity magneto- and electro-metry with long-lived interacting solid-state spins. As a proof of principle, we present an orientation and microwave-free magnetometer based on cross-relaxation.

The electronic spin properties of the negatively charged nitrogen-vacancy (NV^-) center in diamond have given rise to a wealth of applications in nanoscale sensing and quantum information science thanks in part to the possibility to optically polarize and read-out its spin state under ambient conditions [1]. In particular, ensembles of NV centers are widely studied for their enhanced magnetic field sensing capabilities [2–7] and as pristine platforms for observing many-body effects [8–11]. When the NV spin concentration reaches ppm values, spin depolarisation, or cross-relaxation (CR) takes place through a very rich many-body dynamics associated with disorder [12]. These mechanisms limit the efficiency of typical microwave based NV magnetometers, but quantum control techniques can be combined to surpass this interaction limit [13]. Further, CR mechanisms can be turned as a tool for magnetic field sensing [14, 15]. Spectral features in the photoluminescence (PL) indeed appear when the magnetic field crosses specific crystal planes where dipolar interactions are enhanced, leading to CR. The projected sensitivity of such magnetometers lie in the tens of $\mathrm{pT}/\sqrt{\mathrm{Hz}}$ [14], on a par with the most sensitive microwave based NV magnetometers [16, 17].

Cross-relaxation features close to zero magnetic field have also been observed and could be deployed for higher sensitivity microwave-free magnetometry [18, 19]. The CR contrast was indeed shown to be much larger in this zero-field limit [20, 21] but all the relaxation mechanisms have not been identified. Here, we study dipolar relaxation processes in ensembles of NV centers in the presence of small transverse electric and magnetic fields. Specifically, by employing magnetic field scans along specific crystalline directions, we find regimes where flip-flop, double-flip processes as well as mixing induced by local electric fields play a role. We also present an orientation and microwave-free magnetometer that employs double-flip processes in the dipolar interaction between NV centers.

The electronic spin of NV center is a spin-1 system in the electronic ground state (see Fig. 1, top left panel), which can be optically polarized in the $|m_s = 0\rangle$ state. The PL of this state is also larger than in the $|m_s = \pm 1\rangle$ states enabling spin-read out at room temperature [1]. The $|m_s = \pm 1\rangle$ spin states are separated from the $|m_s = 0\rangle$ state by $D = (2\pi)2.87$ GHz so that when a resonant microwave or static transverse magnetic field is applied, the PL is reduced [22, 23]. The processes that lead to depolarisation in strongly coupled spin-1 systems are depicted in Fig. 1. Flip-flop processes involving coupling between spins with identical or different orientations, or "classes", are depicted in the top-right panel. They have already been shown to play a dominant role in dense ensembles of NV centers when $B \gtrsim 30$ G : tuning the difference δ between the different NV centers' spin states indeed result in a strong T_1 reduction [12]. We will show here that double-flip up and down as well as mixing induced by local electric fields (cf. two bottom panels) can also give a significant contribution to the spin depolarization.

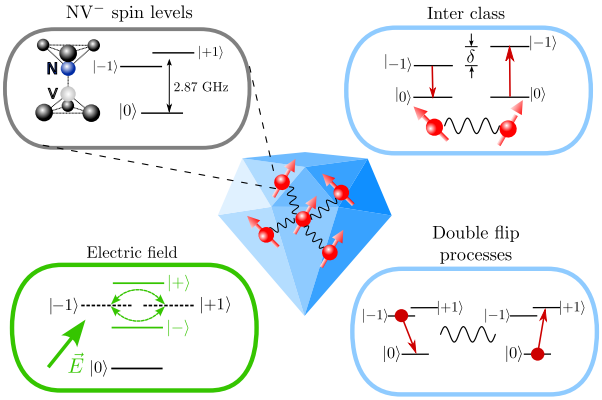

FIG. 1. Schematics showing a diamond with interacting spins (central picture) as well as three processes that account for dipolar relaxation: flip-flop processes involving two different classes of NV centers, local electric field mixing and double-flip processes where two units of spin angular momentum are exchanged.

The experimental apparatus and the samples used in

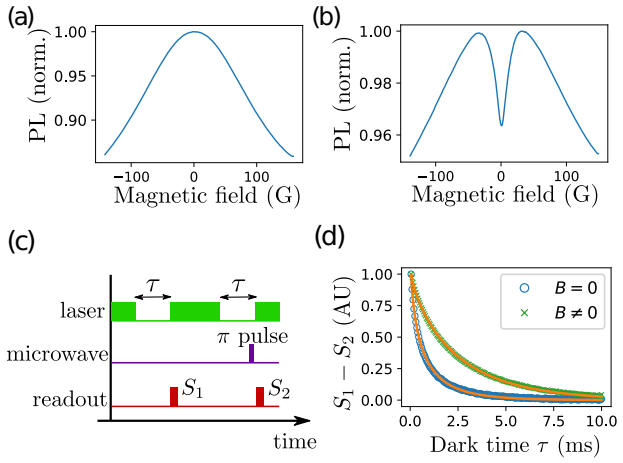

FIG. 2. a) and b) : Photoluminescence from NV center ensembles as a function of a magnetic field applied in an arbitrary direction for sample CVD-1 with [NV$^-$]≈ 50 ppb and for sample HPHT-150-1 with [NV$^-$]≈ 3 ppm respectively. (c) Sequence used to measure the spin lifetime. (d) Trace i) and ii) are the spin relaxation signals $S_1 - S_2$ measured for the dense sample at zero and non-zero magnetic fields respectively. The fitting procedure (orange plain line) is described in the main text.

this study together with their nomenclature are presented in the supplementary material (SM) sec. II and III [24]. Fig. 2-a) and b) show the change in PL as a function of a magnetic field applied *via* a homebuilt electromagnet for two diamond samples with a low and high concentration of NV$^-$ centers respectively (CVD-1 and HPHT-150-1). In both samples, we see a decrease in PL as the magnetic field amplitude increases. There is however a stark difference in the low magnetic field region where only high-density samples shows a drop in PL [20, 21].

This effect has been attributed to CR between the NV centers through dipole-dipole coupling [21, 32]. We will denote T_1^{ph} the characteristic timescale of phonon-induced relaxation and T_1^{dd} the density dependent timescale associated with dipole-dipole interactions. Fig. 2-c) shows the sequence employed to measure T_1 and Fig. 2-d) shows the result of the measurement when $B \approx 0$ and $B \approx 50$ G. All dense samples used in this study show $T_1^{\text{dd}} \sim T_1^{\text{ph}}$ (see SM sec. IV A), so both decay processes are included in the analysis. Fitting the two traces of Fig. 2 d) by the product of a simple and a stretched exponential, we find $T_1^{\text{ph}} = 3.6$ ms for both curves and $T_1^{\text{dd}} = 0.6$ ms and 13.0 ms for trace i) and ii) respectively. These results thus demonstrates a twenty-fold increase in the dipolar depolarization rate when the B field is turned to zero. The fluctuator model developed in [32] contains some of the explanation for this increase in dipolar depolarization: all four NV classes in the diamond are resonant in zero field, which increases the flip-flop rates. However, the model did not include extra specificities in the zero magnetic field region, namely the role of local electric field and double flip processes.

Fig. 3-a) and b)-i) show optically detected magnetic resonance (ODMR) spectra with and without magnetic field, from the dense ensemble HPHT-150-1. From the resonance line-widths in a magnetic field, we extract decoherence rates T_2^* in the hundreds of nanosecond range, limited by the coupling between NV centers and the fluctuating spins of substitutional nitrogen atoms (also called P_1 centers). Using the same magnetic field alignment, Fig. 3 (b)-ii) and iii) show the PL and the $1/T_1^{\text{dd}}$ decay rates from the NV center ensemble as a function of the amplitude of the magnetic field. We observe that the 4 % increase in PL as the magnetic field increases is indeed correlated with a drop in the spin decay rate from 1600 s^{-1} to 80 s^{-1}. This result can again be explained by the decreasing number of resonant spins as the zero magnetic field is increased. We also confirmed that the half width of the dip (≈ 10 G) is consistent with a fluctuator model taking into account the reduction of the two spin resonances overlap as the B field is increased (see SM sec. IV C).

Fig. 3 (c)-i) instead shows an ODMR where all four classes are brought to resonance by placing the magnetic field along the [100] crystalline axis. Fig. 3 (c)-ii) and (c)-iii) show the change in the PL and in $1/T_1^{\text{dd}}$ as a function of a magnetic field that is aligned in this direction. Surprisingly, we can still observe an increase in the spin decay rate and a corresponding drop in the PL when the magnetic field tends to zero, although all classes are always resonant (see SM, sec. IV-E). We also note that the PL and $1/T_1^{\text{dd}}$ change is also much sharper in this scenario.

When $\gamma|\mathbf{B}| \gg 1/T_2^*$, the only resonant terms in the dipole-dipole coupling between NV centers are the flip-flop terms $|0,\pm1\rangle\langle\pm1,0|$ (see SM sec. V). In zero magnetic field however, other resonant mechanisms of the dipolar Hamiltonian have to be taken into consideration, which may elucidate the above result. It was shown in [33] that local electric fields coming from P_1^+ or NV$^-$ centers are responsible for ODMR profiles at zero magnetic field. In order to estimate their contributions in the spin relaxation, we perform numerical simulations where we add the following Hamiltonian for the electric field dependent NV$^-$ ground state:

$$\mathcal{H}_{\text{elec}} = d_\perp \left[E_x(\hat{S}_y^2 - \hat{S}_x^2) + E_y(\hat{S}_x\hat{S}_y + \hat{S}_y\hat{S}_x) \right]. \quad (1)$$

$E_{x,y}$ are the projections of local electric fields on the NV axes and $d_\perp = 17$ Hz · cm/V is the transverse electric field susceptibility. Under local electric fields with orientations given by the angle $\phi_E = \tan(E_x/E_y)$, the eigenstates of the total hamiltonian of the NV spins in the ground state are $|0\rangle$ and $|\pm\rangle = \frac{1}{\sqrt{2}}(|+1\rangle \pm e^{-i\phi_E}|-1\rangle)$. Computing the influence of the flip-flop terms $|\pm,0\rangle\langle0,\pm|$ in the fluctuator model shows that $1/T_1^{\text{dd}}$ indeed increases at zero field, even after averaging over all possible angles ϕ_E (see SM, sec. V-E). Another mechanism at stake when considering dipolar interactions between spin-1 systems at low fields are double-flip processes. These

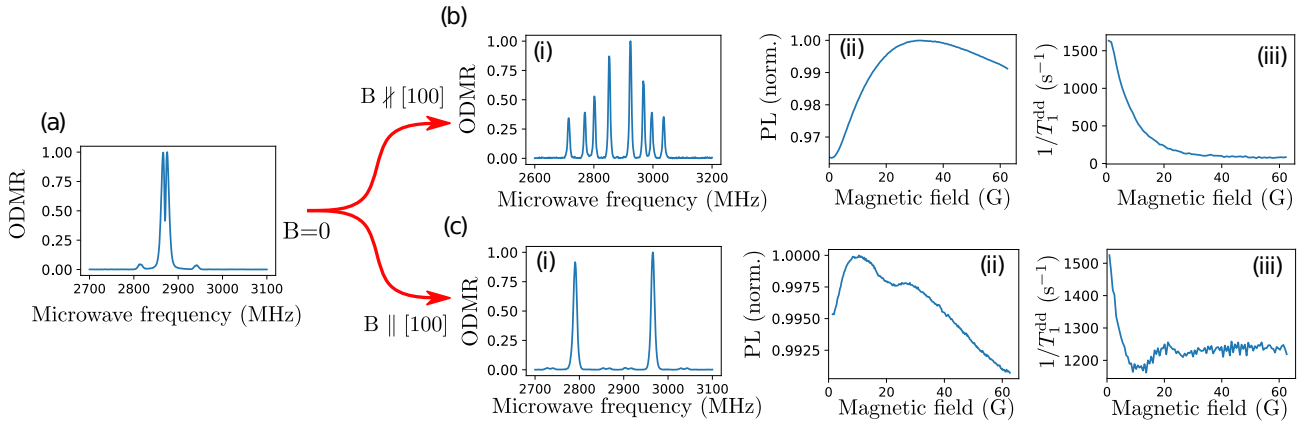

FIG. 3. (a) ODMR spectrum in zero field with microwave amplitude modulation (see experimental details in SM sec. III). (b)-i) ODMR spectrum for a magnetic field ≈ 60 G, misaligned by $\sim 24°$ from the [100] axis. (b)-ii) Normalized PL of the NV^- ensemble as a function of the magnetic field amplitude. (b)-iii) Stretched part of the spin decay $1/T_1^{dd}$ as a function of the magnetic field amplitude. (c)-i), (c)-ii) and (c)-iii): same measurements as (b) but with a magnetic field close to the [100] axis. All the measurements were realized using the sample HPHT-150-1.

processes correspond to the terms $|+1,0\rangle\langle 0,-1|$ in the dipolar interaction, giving rise to an exchange of two units of spin-angular momentum when the $|\pm1\rangle$ states are resonant. Simulations (see SM, sec V-F) suggest that double-flips contribute significantly to the spin relaxation at low fields.

To quantify these two processes experimentally, we apply a purely transverse magnetic field on one of the NV class. Indeed, when $B_\perp \leq 150$ G, the eigenstates of the spin Hamiltonian are close to $|0\rangle$, $|+\rangle$ and $|-\rangle$ to $\approx 2\%$ (see SM sec. IV-F). We can thus use the transverse field to emulate the role of the electric field, a property that has previously been used to increase the electric field sensing ability of NV centers [34, 35]. Fig. 4 (a) shows an ODMR spectrum where $B_\perp = 20$ G on sample HPHT-150-2. The central two lines correspond to the $|0\rangle \rightarrow |-\rangle$ and $|0\rangle \rightarrow |+\rangle$ transitions for the class that is orthogonal to $\boldsymbol{B}$. Fig. 4-(c) shows the measurement of the decay rate $1/T_1^{dd}$ for that class, as a function of $B_\perp$. Two regions can be observed on this graph: in region A the decay rate decreases with $B_\perp$, while in region B it stabilizes to a value $1/T_1^{dd} = 60 \pm 5$ s^{-1}. We also indicated the value $1/T_1^{dd} = 25 \pm 5$ s^{-1} found for the same class but employing a longitudinal magnetic field.

To understand these results, we plot the detuning $\Delta\nu$ between the states $|+\rangle$ and $|-\rangle$ as a function of $B_\perp$ in Fig. 4 (b). When $\delta\nu > 1/T_2^*$, these states do not overlap any longer, so we can interpret our results as follows: double-flips are efficient in region A, up to a point where state overlap is negligible. In region B, only the flip-flops in the basis $|\pm\rangle$ play a role. We note that the decay rate in the $\{|0\rangle, |\pm\rangle\}$ basis is more than a factor of two larger than the decay rate coming from intra-class flip-flops in the $\{|0\rangle, |\pm1\rangle\}$ basis. This effect is corroborated by our model detailed in SM sec. V. Importantly, in region A, the double-flips processes give a maximum decay rate that is ~ 5 times greater than the decay caused by the change of basis alone. From these results and according to our model, the double-flips are thus the dominant cause of zero-field depolarization observed in Fig. 3 (c)-iii).

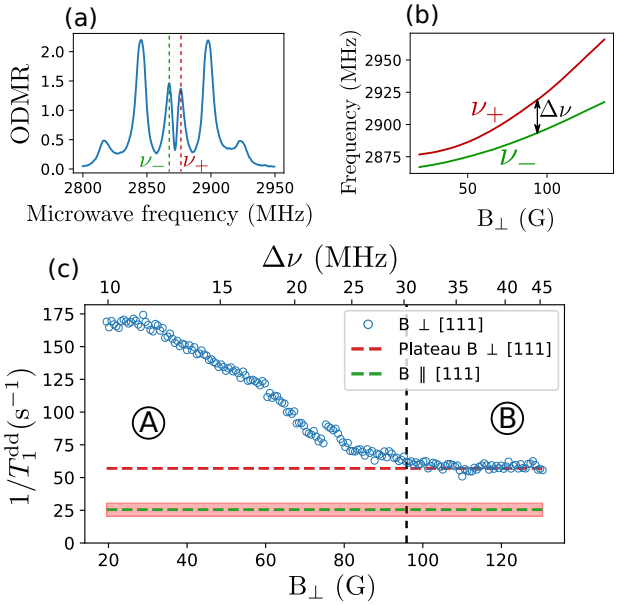

FIG. 4. (a) ODMR spectrum for $B_\perp = 20$ G. The two transition frequencies of the class that is orthogonal to B are denoted ν_+ and ν_-. (b) Measurement of ν_+ and ν_- through ODMR as a function of $B_\perp$. (c) Measurement of $1/T_1^{dd}$ for a single NV class as a function of $B_\perp$. The red dashed line is the value reached for high transverse field. The green dashed line correspond to the value found for the same sample and NV class, under a longitudinal magnetic field. Error bars are depicted by the shaded pink region. The detuning $\Delta\nu = \nu_+ - \nu_-$ is indicated on the top x-axis. Vertical black dashed line indicates the separation between regions A and B (see main text).

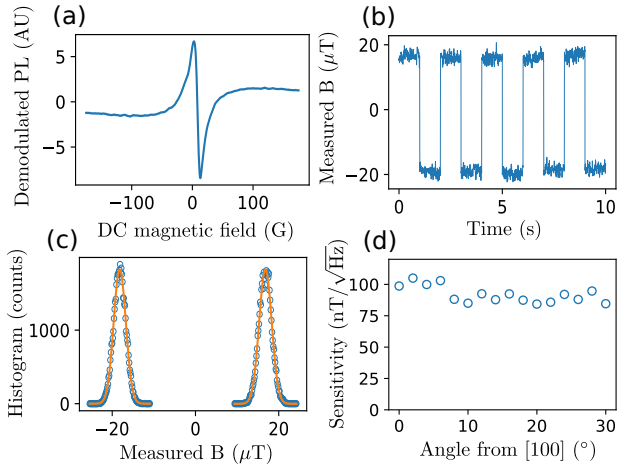

FIG. 5. Low-field magnetometry protocol. (a) Demodulated PL as a function of an externally applied magnetic field. (b) External magnetic field read-out. (c) Histogram of the measurement in Fig. (b) fitted by gaussians of standard deviation $\sigma = 1.5$ μT. (d) Measured sensitivity as function of the angle between the external magnetic field and the [100] crystalline axis.

Our observations have important implications for magnetometry with NV ensembles. DC microwave-free magnetometry has already been performed using either NV-NV cross-relaxations [14, 15] or level anti-crossing [36–38]. Here we propose a similar protocol but using the spin depolarization at zero-field. To do so, we use a lock-in detection and add a magnetic field modulation at ~ 1 kHz with an amplitude ~ 10 G through the same electromagnet. Fig. 5-(a) shows the demodulated PL while a DC magnetic field is scanned in an arbitrary direction. Here, we use the sample HPHT-15-1 with a laser power ~ 1 mW. The optical power in the collected PL is ~ 1 μW. We can see a sharp linear slope in low field $|B| < 5$ G. Once calibrated, the slope provides a 1D magnetometer, which could be extended to 3D with a set of 3 coils or 3 electromagnets, as in [38]. In order to assess the sensitivity of the measurement, we alternate a small DC field of ≈ 40 μT every few seconds and take a histogram of the measured fields (with a total duration of ≈50 s), as shown in Fig. 5-(b) and (c). The histogram is well fitted by gaussians of standard deviation $\sigma = 1.5$ μT. The measurement was performed here with an output low-pass filter of time constant $\tau = 3$ ms, which gives us a DC sensitivity $\eta = \sigma\sqrt{\tau} = 82$ nT/$\sqrt{\text{Hz}}$. This value corresponds to $\eta/\sqrt{V} \approx 4.7$ $\mu\text{T}/\mu\text{m}^{3/2}/\sqrt{\text{Hz}}$ when normalized to the volume. Importantly, this measurement is consistent with the experimentally found ~ 5 $\mu\text{T}/\sqrt{\text{Hz}}$ sensitivity obtained with sample HPHT-1-1 (see samples details in SM sec. II).

Our results implies bright perspectives for high-sensitivity magnetometry using NV centers in a millimeter size volumes. Furthermore, compared to previously employed protocols, the sensitivity does not crucially depend on crystalline orientation, making this magnetometer principle operational with diamond powders or polycrystalline samples. Another significant advantage is that this measurement is insensitive to thermal fluctuations and strain inhomogeneities because dipolar-relaxation at zero-field does not depend on the zero-field splitting. In other typical NV magnetometers however, the zero-field splitting dependence with temperature and strain can give systematic errors [6, 7].

We now evaluate the relative role of the three causes of spin depolarization that assist the operation of the magnetometer. To do so, we measure its sensitivity while changing the angle of the magnetic field. The results are shown in Fig. 5 (d). We observe only a $\sim 10\%$ improvement in the sensitivity as we leave the [100] region. When $\boldsymbol{B} \parallel$ [100] only the double flips and the electric field cause a depolarization, whereas the three effects are at play in all the other orientations. It should be noted that this observation is sample dependent. Other samples, including those from the same batch, have shown a higher orientation dependence, corresponding to a lower contribution from local electric fields and double-flip processes. Interestingly, the double-flips and electric field effects are here the dominant factors in the sensitivity of this protocol.

As a conclusion, we identified three mechanisms causing spin depolarization in zero field for dense ensemble of NV^- centers, all related to an increase in the dipole-dipole induced CR between the spins of NV centers. The lift in degeneracy of the spin state of different NV classes was found to be the main cause of zero-field depolarization, followed by double-flip processes and then the electric field induced mixing. We have employed CR for microwave and orientation-free DC-magnetometry and demonstrated a sensitivity below 100 nT/$\sqrt{\text{Hz}}$ for a single 15 μm diameter commercially available diamond and show that that double-flips and local electric fields play a critical role. We believe that our results will also be important for microwave-based low field magnetometry [39, 40] and for understanding many-body phenomena [8–11] and spin-mechanical effects [41] with strongly coupled spins under purely transverse or small magnetic fields.

ACKNOWLEDGMENTS

We would like to acknowledge support from Alexandre Tallaire and Jocelyn Achard as well as SIRTEQ for funding.

[1] M. W. Doherty, N. B. Manson, P. Delaney, F. Jelezko, J. Wrachtrup, and L. C. Hollenberg, Physics Reports **528**, 1 (2013), the nitrogen-vacancy colour centre in di-

amond.
[2] V. M. Acosta, E. Bauch, M. P. Ledbetter, C. Santori, K.-M. C. Fu, P. E. Barclay, R. G. Beausoleil, H. Linget, J. F. Roch, F. Treussart, S. Chemerisov, W. Gawlik, and D. Budker, Phys. Rev. B **80**, 115202 (2009).
[3] A. Tallaire, O. Brinza, P. Huillery, T. Delord, C. Pellet-Mary, R. Staacke, B. Abel, S. Pezzagna, J. Meijer, N. Touati, L. Binet, A. Ferrier, P. Goldner, G. Hetet, and J. Achard, Carbon **170**, 421 (2020).
[4] A. M. Edmonds, C. A. Hart, M. J. Turner, P.-O. Colard, J. M. Schloss, K. S. Olsson, R. Trubko, M. L. Markham, A. Rathmill, B. Horne-Smith, *et al.*, Materials for Quantum Technology **1**, 025001 (2021).
[5] G. Chatzidrosos, J. S. Rebeirro, H. Zheng, M. Omar, A. Brenneis, F. M. Stürner, T. Fuchs, T. Buck, R. Rölver, T. Schneemann, *et al.*, Frontiers in Photonics , 4 (2021).
[6] J. F. Barry, J. M. Schloss, E. Bauch, M. J. Turner, C. A. Hart, L. M. Pham, and R. L. Walsworth, Rev. Mod. Phys. **92**, 015004 (2020).
[7] E. Bauch, C. A. Hart, J. M. Schloss, M. J. Turner, J. F. Barry, P. Kehayias, S. Singh, and R. L. Walsworth, Phys. Rev. X **8**, 031025 (2018).
[8] G. Kucsko, S. Choi, J. Choi, P. C. Maurer, H. Zhou, R. Landig, H. Sumiya, S. Onoda, J. Isoya, F. Jelezko, *et al.*, Physical review letters **121**, 023601 (2018).
[9] S. Choi, J. Choi, R. Landig, G. Kucsko, H. Zhou, J. Isoya, F. Jelezko, S. Onoda, H. Sumiya, V. Khemani, C. von Keyserlingk, N. Y. Yao, E. Demler, and M. D. Lukin, Nature **543**, 221 (2017).
[10] C. Zu, F. Machado, B. Ye, S. Choi, B. Kobrin, T. Mittiga, S. Hsieh, P. Bhattacharyya, M. Markham, D. Twitchen, A. Jarmola, D. Budker, C. R. Laumann, J. E. Moore, and N. Y. Yao, Nature **597**, 45 (2021).
[11] B. L. Dwyer, L. V. Rodgers, E. K. Urbach, D. Bluvstein, S. Sangtawesin, H. Zhou, Y. Nassab, M. Fitzpatrick, Z. Yuan, K. De Greve, *et al.*, arXiv preprint arXiv:2103.12757 (2021).
[12] S. Choi, J. Choi, R. Landig, G. Kucsko, H. Zhou, J. Isoya, F. Jelezko, S. Onoda, H. Sumiya, V. Khemani, C. von Keyserlingk, N. Y. Yao, E. Demler, and M. D. Lukin, Nature **543**, 221 (2017), number: 7644 Publisher: Nature Publishing Group.
[13] H. Zhou, J. Choi, S. Choi, R. Landig, A. M. Douglas, J. Isoya, F. Jelezko, S. Onoda, H. Sumiya, P. Cappellaro, *et al.*, Physical review X **10**, 031003 (2020).
[14] R. Akhmedzhanov, L. Gushchin, N. Nizov, V. Nizov, D. Sobgayda, I. Zelensky, and P. Hemmer, Phys. Rev. A **96**, 013806 (2017), number: 1.
[15] R. Akhmedzhanov, L. Gushchin, N. Nizov, V. Nizov, D. Sobgayda, I. Zelensky, and P. Hemmer, Phys. Rev. A **100**, 043844 (2019), number: 4.
[16] T. Wolf, P. Neumann, K. Nakamura, H. Sumiya, T. Ohshima, J. Isoya, and J. Wrachtrup, Phys. Rev. X **5**, 041001 (2015).
[17] F. M. Stürner, A. Brenneis, T. Buck, J. Kassel, R. Rölver, T. Fuchs, A. Savitsky, D. Suter, J. Grimmel, S. Hengesbach, M. Förtsch, K. Nakamura, H. Sumiya, S. Onoda, J. Isoya, and F. Jelezko, Advanced Quantum Technologies **4**, 2000111 (2021), https://onlinelibrary.wiley.com/doi/pdf/10.1002/qute.202000111.
[18] D. Filimonenko, V. Yasinskii, A. Nizovtsev, and S. Y. Kilin, Semiconductors **52**, 1865 (2018).
[19] D. Filimonenko, V. Yasinskii, A. P. Nizovtsev, S. Y. Kilin, and F. Jelezko, Journal of Applied Spectroscopy **88**, 1131 (2022).
[20] A. Jarmola, A. Berzins, J. Smits, K. Smits, J. Prikulis, F. Gahbauer, R. Ferber, D. Erts, M. Auzinsh, and D. Budker, Appl. Phys. Lett. **107**, 242403 (2015), number: 24.
[21] M. Mrózek, D. Rudnicki, P. Kehayias, A. Jarmola, D. Budker, and W. Gawlik, EPJ Quantum Technol. **2**, 22 (2015), number: 1.
[22] R. Epstein, F. Mendoza, Y. Kato, and D. Awschalom, Nature physics **1**, 94 (2005).
[23] N. D. Lai, D. Zheng, F. Jelezko, F. Treussart, and J.-F. Roch, Applied Physics Letters **95**, 133101 (2009).
[24] See supplemental material at [...], which includes refs. [25-31].
[25] S. Anishchik, V. Vins, A. Yelisseyev, N. Lukzen, N. Lavrik, and V. Bagryansky, New Journal of Physics **17**, 023040 (2015).
[26] D. Filimonenko, V. Yasinskii, A. Nizovtsev, S. Y. Kilin, and F. Jelezko, Semiconductors **54**, 1730 (2020).
[27] E. Van Oort and M. Glasbeek, Chemical Physics Letters **168**, 529 (1990).
[28] R. Giri, F. Gorrini, C. Dorigoni, C. E. Avalos, M. Cazzanelli, S. Tambalo, and A. Bifone, Phys. Rev. B **98**, 045401 (2018), number: 4.
[29] R. Giri, C. Dorigoni, S. Tambalo, F. Gorrini, and A. Bifone, Phys. Rev. B **99**, 155426 (2019), number: 15.
[30] L. T. Hall, P. Kehayias, D. A. Simpson, A. Jarmola, A. Stacey, D. Budker, and L. C. L. Hollenberg, Nature Communications **7**, 10211 (2016).
[31] A. Jarmola, V. M. Acosta, K. Jensen, S. Chemerisov, and D. Budker, Phys. Rev. Lett. **108**, 197601 (2012), number: 19.
[32] J. Choi, S. Choi, G. Kucsko, P. C. Maurer, B. J. Shields, H. Sumiya, S. Onoda, J. Isoya, E. Demler, F. Jelezko, *et al.*, Physical review letters **118**, 093601 (2017).
[33] T. Mittiga, S. Hsieh, C. Zu, B. Kobrin, F. Machado, P. Bhattacharyya, N. Rui, A. Jarmola, S. Choi, D. Budker, *et al.*, Physical review letters **121**, 246402 (2018).
[34] F. Dolde, H. Fedder, M. W. Doherty, T. Nöbauer, F. Rempp, G. Balasubramanian, T. Wolf, F. Reinhard, L. C. Hollenberg, F. Jelezko, *et al.*, Nature Physics **7**, 459 (2011).
[35] Z. Qiu, A. Hamo, U. Vool, T. X. Zhou, and A. Yacoby, arXiv preprint arXiv:2205.03952 (2022).
[36] A. Wickenbrock, H. Zheng, L. Bougas, N. Leefer, S. Afach, A. Jarmola, V. M. Acosta, and D. Budker, Applied Physics Letters **109**, 053505 (2016), https://doi.org/10.1063/1.4960171.
[37] H. Zheng, G. Chatzidrosos, A. Wickenbrock, L. Bougas, R. Lazda, A. Berzins, F. H. Gahbauer, M. Auzinsh, R. Ferber, and D. Budker, in *Slow Light, Fast Light, and Opto-Atomic Precision Metrology X*, Vol. 10119 (SPIE, 2017) pp. 115–122.
[38] H. Zheng, Z. Sun, G. Chatzidrosos, C. Zhang, K. Nakamura, H. Sumiya, T. Ohshima, J. Isoya, J. Wrachtrup, A. Wickenbrock, and D. Budker, Phys. Rev. Applied **13**, 044023 (2020), number: 4.
[39] P. J. Vetter, A. Marshall, G. T. Genov, T. F. Weiss, N. Striegler, E. F. Großmann, S. Oviedo-Casado, J. Cerrillo, J. Prior, P. Neumann, and F. Jelezko, Phys. Rev. Applied **17**, 044028 (2022).
[40] N. Wang, C.-F. Liu, J.-W. Fan, X. Feng, W.-H. Leong, A. Finkler, A. Denisenko, J. Wrachtrup, Q. Li, and R.-B. Liu, Phys. Rev. Research **4**, 013098 (2022).

[41] C. Pellet-Mary, P. Huillery, M. Perdriat, and G. Hétet, Physical Review B **104**, L100411 (2021).